S33A-2509

Rupture Processes of the 2011 Tohoku Earthquake and the 2011 Ibaraki-Oki Earthquake

Hisahiko Kubo[1], Kimiyuki Asano [1], Tomotaka Iwata [1], Yasumaro Kakehi [2]
[1] DPRI, Kyoto Univ., Uji, Kyoto, Japan, [2] Grad. Sch. of Science, Kobe Univ., Kobe, Hyogo, Japan
E-mail: kubo.hisahiko.26a@st.kyoto-u.ac.jp

Abstract

At 14:46:18 on March 11 2011 (JST; 05:46 on 11 March, UTC), the Tohoku earthquake (Mw 9.1) occurred off the Pacific coast of Northeastern Japan (off Tohoku region, Japan). Approximately 29 minutes after this event (at 15:15:34), the Ibaraki-Oki earthquake (Mw 7.9) occurred off the southernmost portion of the northeastern Japan (off Ibaraki Prefecture, Kanto, Japan).

In this study, we estimate the rupture process of the 2011 Tohoku earthquake from the joint inversion of teleseismic body waves and geodetic data with enhanced reliability by using objectively determined inversion settings: the maximum slip duration of each subfault (Tsd) and the propagation velocity of the first time window (Vftw). We also estimate the rupture process of the 2011 Ibaraki-Oki earthquake focusing on the relationship of the fault rupture with the subducted seamount and the Philippine Sea plate (PHS). Then, we discuss the relationship between the 2011 Tohoku earthquake and the 2011 Ibaraki-Oki earthquake.

■ Modified figure from GCMT web page

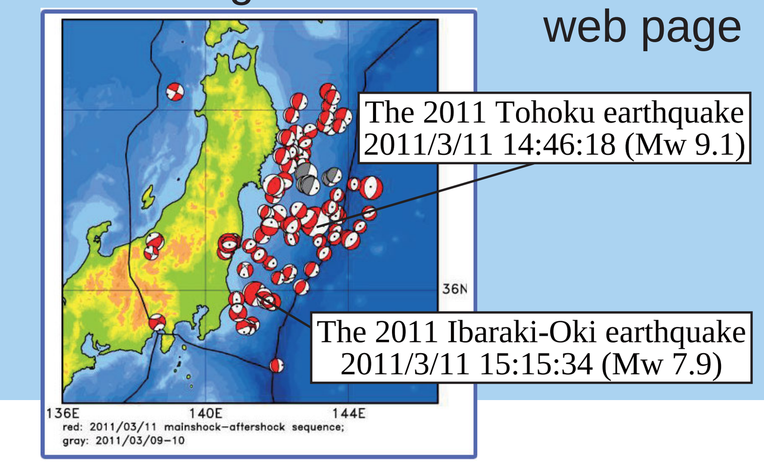

The 2011 Tohoku earthquake

Here, we focus on two important inversion settings in the multiple time window analysis (Hartzell and Heaton, 1983): the maximum slip duration at each subfault (Tsd) and the propagation velocity of the first time window (Vftw). Tsd and Vftw are the parameters controlling the slip time at each subfault and have a significant influence on the estimated source model. Therefore, if the assumed values of Tsd and Vftw are not appropriate, the estimated solution would be distorted. However, as for Tsd, the reason for adopting that value was rarely mentioned in the previous studies. The choice of its value is depending on the analyzer and there is no objective criterion for selecting an adequate value for it. As for Vftw, an approach selecting the value giving the minimum residual between the observed and synthetic waveforms was usually adopted in the previous studies. However, it is difficult to choose the adequate value of Vftw from the waveform fitting of the teleseismic body waves alone because a strong trade-off exists between this parameter and the slip distribution. Consequently, it is frequently seen that various values are adopted depending on analyzers for a common earthquake. This would be one reason that although many source studies for the 2011 Tohoku earthquake have already been published, the obtained source models in these studies differ in various points. In this study, we select the values of these two parameters as objectively as possible based on approaches using data other than the teleseismic body waves. It will enhance objectivity of the inverted slip model.

As space is limited here, the inversion detail and the data fitting of the analysis for the 2011 Tohoku earthquake are written on the backside of the handout, whcih can also be found in Kubo and Kakehi (2013).

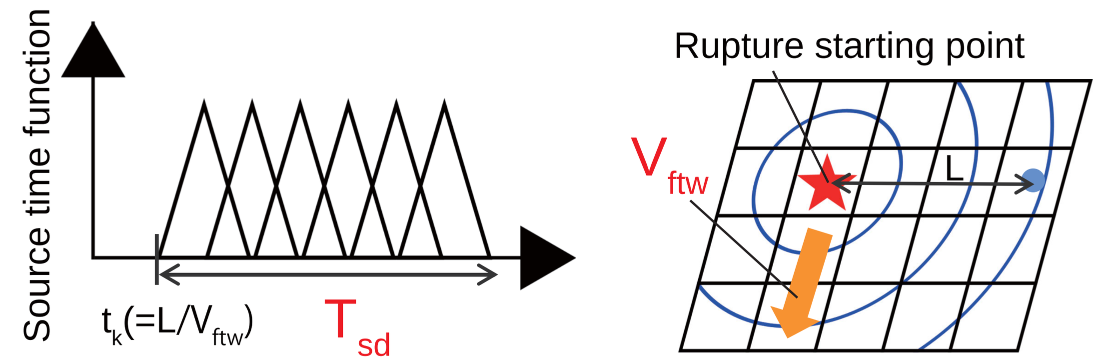

Effects of Tsd and Vftw

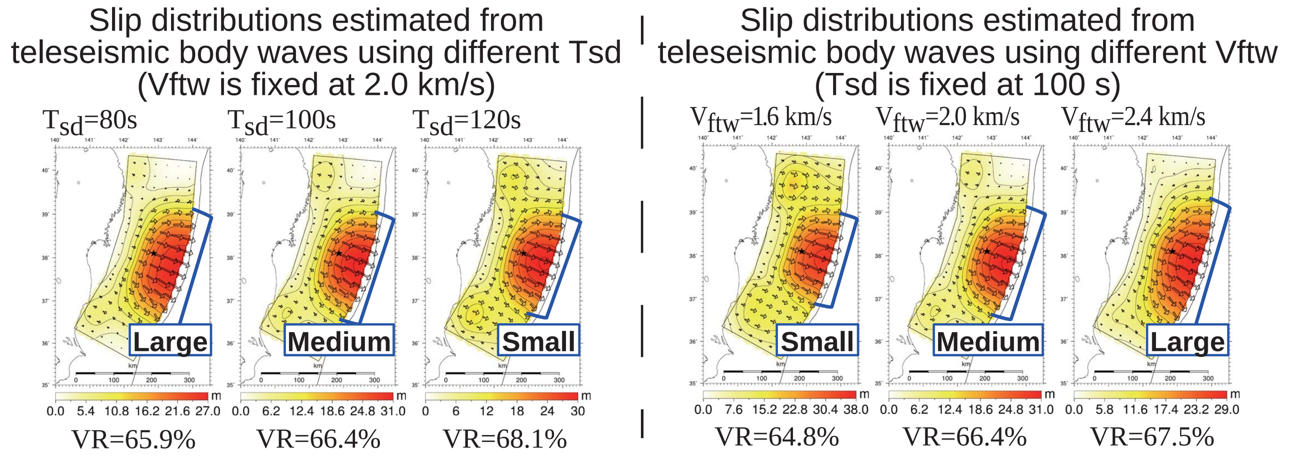

- The inverted source model is significantly affected by the choice of the values of Tsd and Vftw in the teleseismic inversion.
- It is difficult to choose the adequate values of Tsd and Vftw from the waveform fitting of the teleseismic body waves alone.

Determination of Tsd and Vftw

For determining Tsd, we performed semblance analysis of the near-source small-aperture seismic array data of the strong ground motion waveforms to estimate the wave-radiation duration from the area around the hypocenter. From the result of this analysis, we adopted 100 s as Tsd.

As for Vftw, we adopted 2.0 km/s from the matching of the slip patterns of the teleseismic model and the geodetic model. In this analysis, the spatial resolution of geodetic inversion is significantly improved by using seafloor crustal deformation data (Sato et al., 2011) in addition to terrestrial GPS data.

Example of Sembalance Analysis

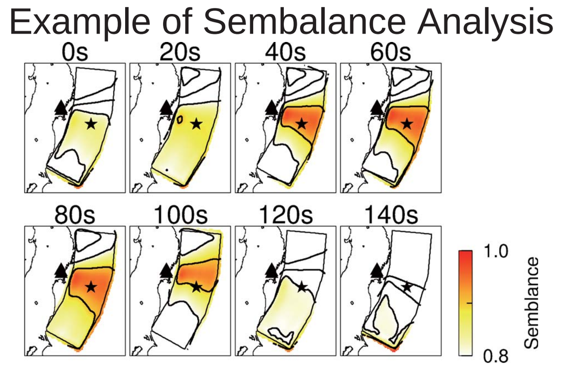

Concept for Determining Vftw

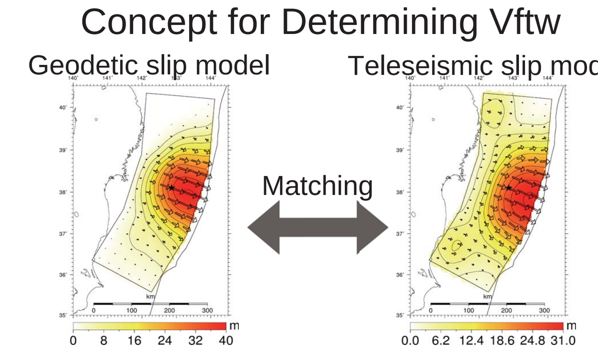

Result & Discussion

■ Slip distribution

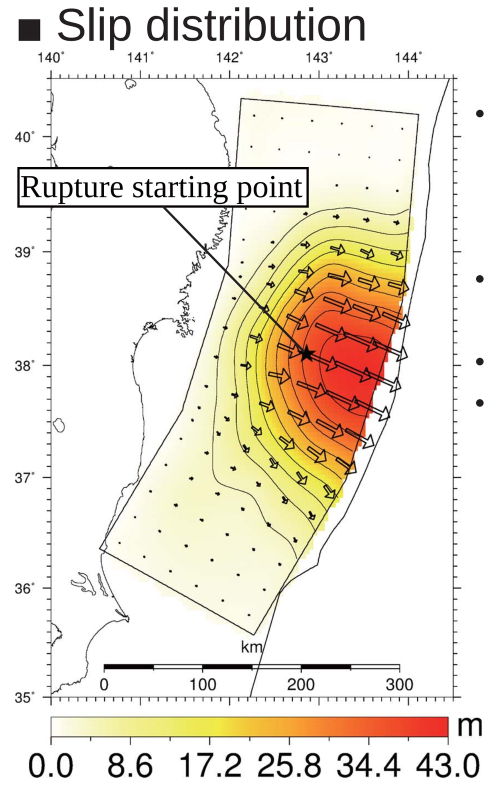

- Large slip is found in the shallow part of the fault surface including the hypocenter.
- Seismic Moment: 1.4×10^{22}Nm (M_W 9.0)
- Maximum slip : 43.0m.
- Total rupture duration: ~150 s

■ Snapshots of the rupture propagation (12 s time step)

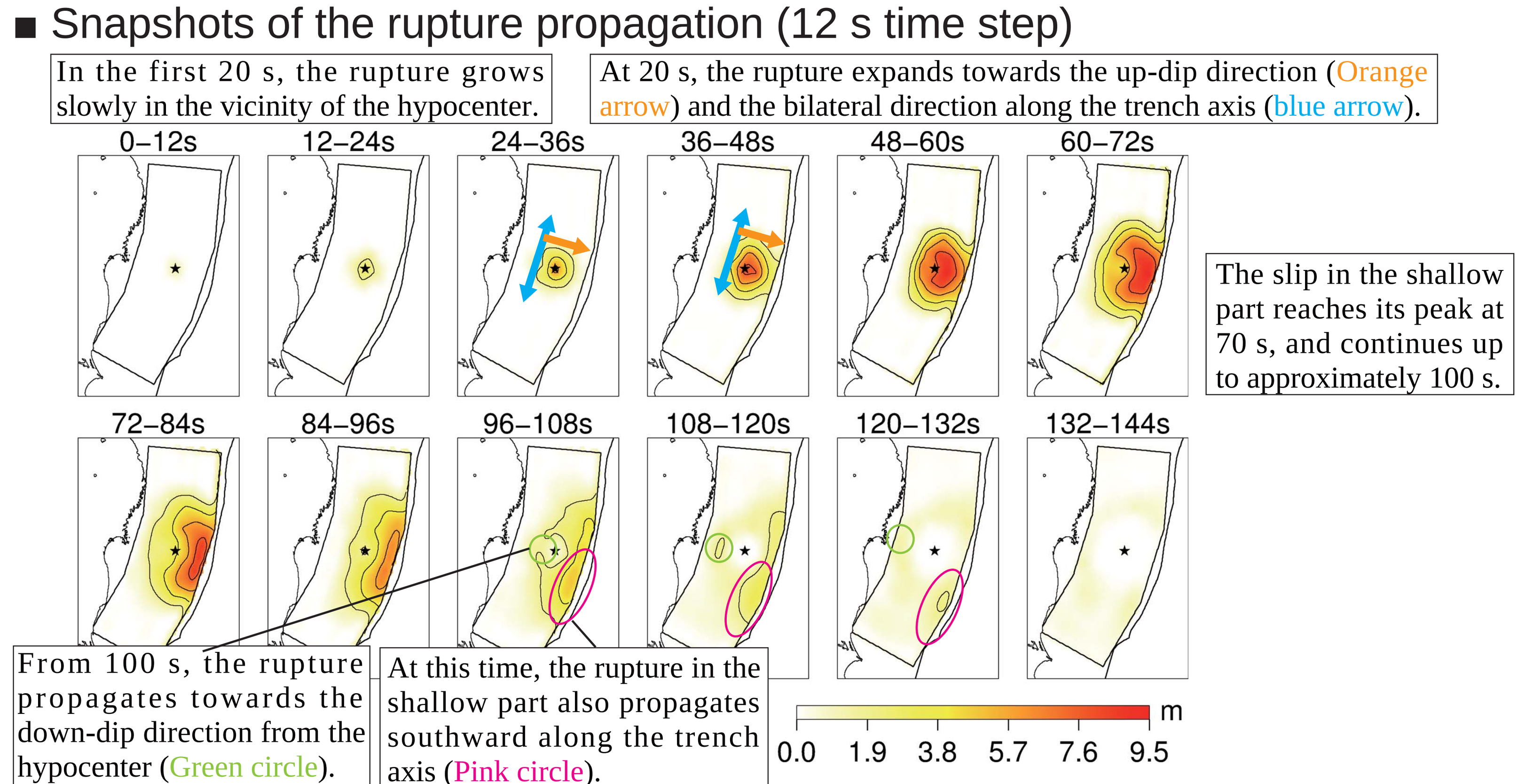

■ Slip rate function at each subfault

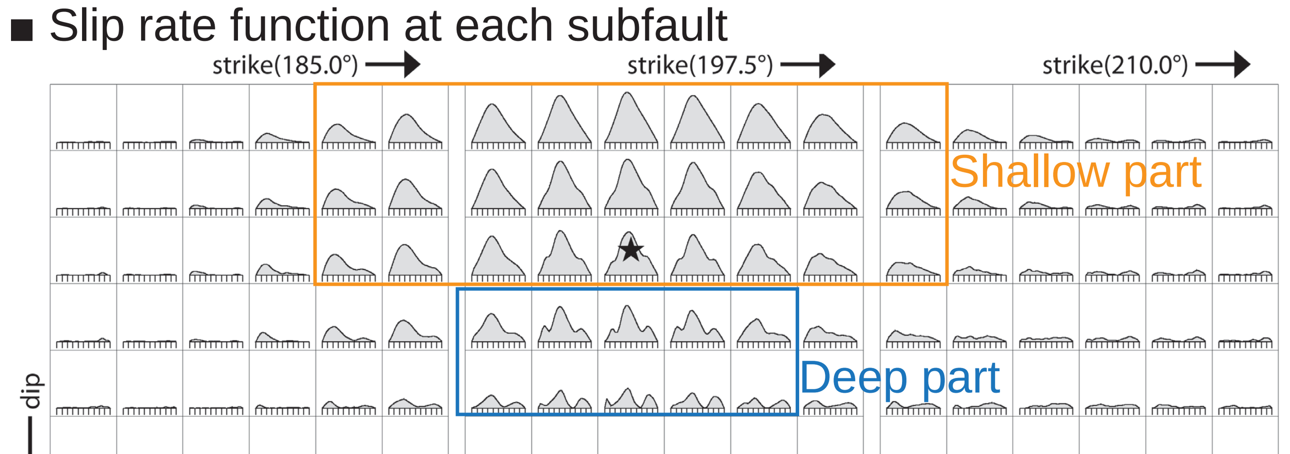

* Slip rate function is derived from the source time function with the rigidity model constructed for subfaults with different locations along dip direction, neglecting the finiteness of the subfault.

The slip behavior in shallow part is different from that in deep part: the slip rate function in shallow part has one peak and its duration is long (Orange), while the slip rate function in deep part has two or three peaks (Blue). This indicates that the rupture property in suduction zone varies along the dip direction (e.g., Lay et al., 2012). The complexity of the slip rate function in deep part may have a relationship with SMGA (strong motion generation area) model that two SMGAs are identified at deep side of the hypocenter (e.g., Asano and Iwata, 2012).

■ Comparison with SMGA model

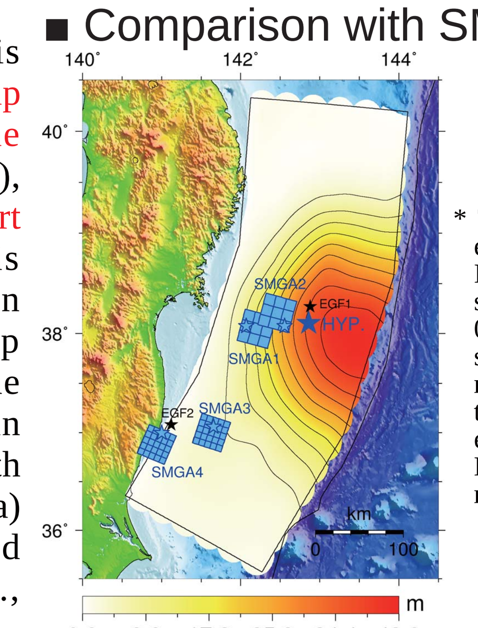

* The SMGA model is estimated by Asano and Iwata (2012) based on strong-motion data in 0.1-10 s. The large and small solid stars represent epicenters of the 2011 Tohoku earthquake and two EGF events by JMA, respectively.

The 2011 Ibaraki-Oki earthquake

At approximately 70 km east-southeast from the epicenter of the 2011 Ibaraki-Oki earthquake, Mochizuki et al. (2008) found a subducting seamount (Purple broken circle). In addition, the plate overlying PAC changes from NA in the north of Kanto to the Philippine Sea plate (PHS) in the south. Uchida et al. (2009) estimated the border between the two overlying plates (the northeastern edge of the PHS) (Blue broken line). Seamount has been thought to have a significant effect on fault rupture and a large number of studies have been made on this topic (e.g. Scholz and Small, 1991; Mochizuki et al, 2008); however, only few attempts regarding how seamount works during the fault rupture have so far been made. Little attention has been given to the relationship between the fault rupture of interplate earthquake and nearby other plate. Therefore, the analysis of the 2011 Ibaraki-Oki earthquake is a good opportunity to understand how seamount and other plate affect the fault rupture of interplate earthquake.

The inversion detail and the data fitting of the analysis for the 2011 Ibaraki-Oki earthquake are also written on the backside of the handout.

Result & Discussion

■ Slip distribution

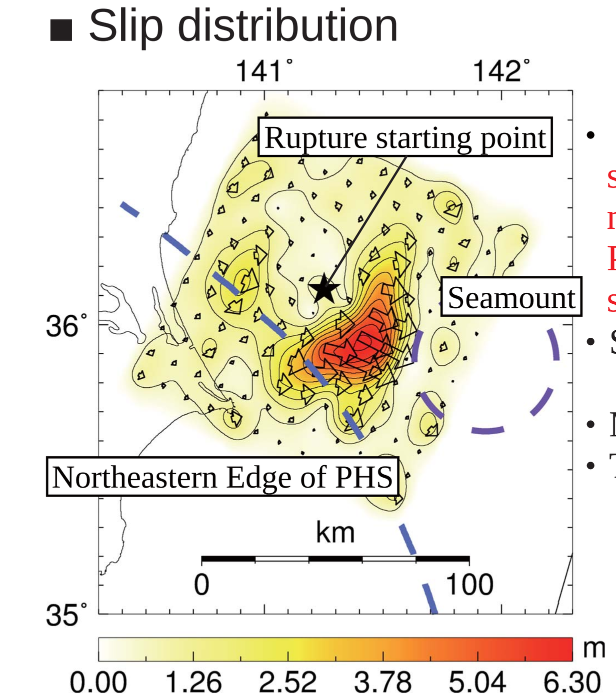

- Large slip area is surrounded by the northeastern edge of PHS and the subducted seamount.
- Seismic moment: 2.8×10^{20}Nm (M_W 7.9)
- Maximum slip: 6.3m
- Total rupture duration: ~30 s.

■ Snapshots of the rupture propagation (5 s time step)

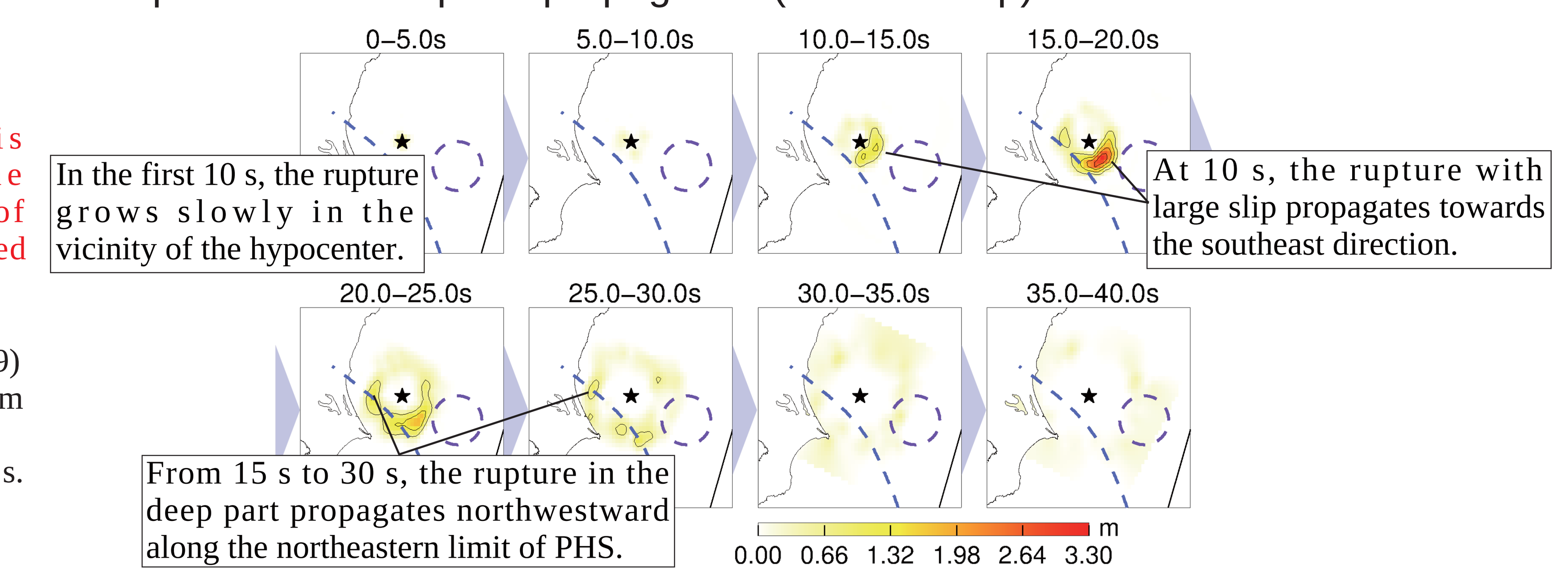

■ Slip rate function at each subfault

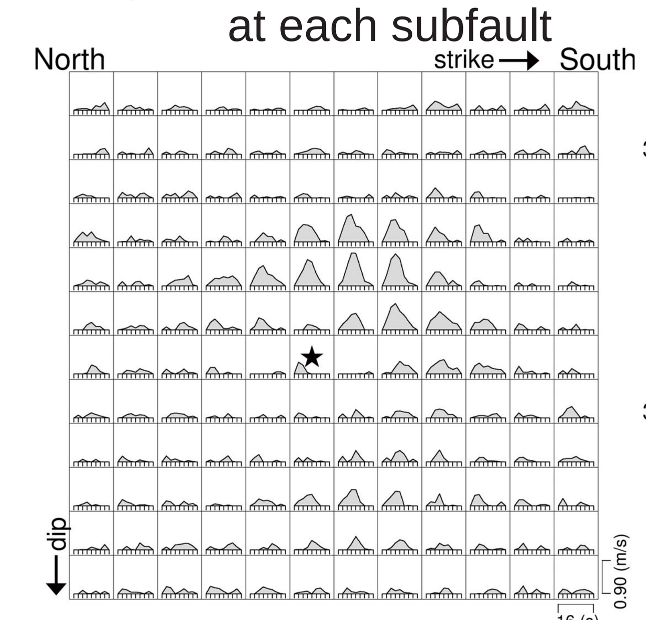

■ Comparison with the spatial distribution of interplate earthquake before and after the 2011 Ibaraki-Oki earthquake

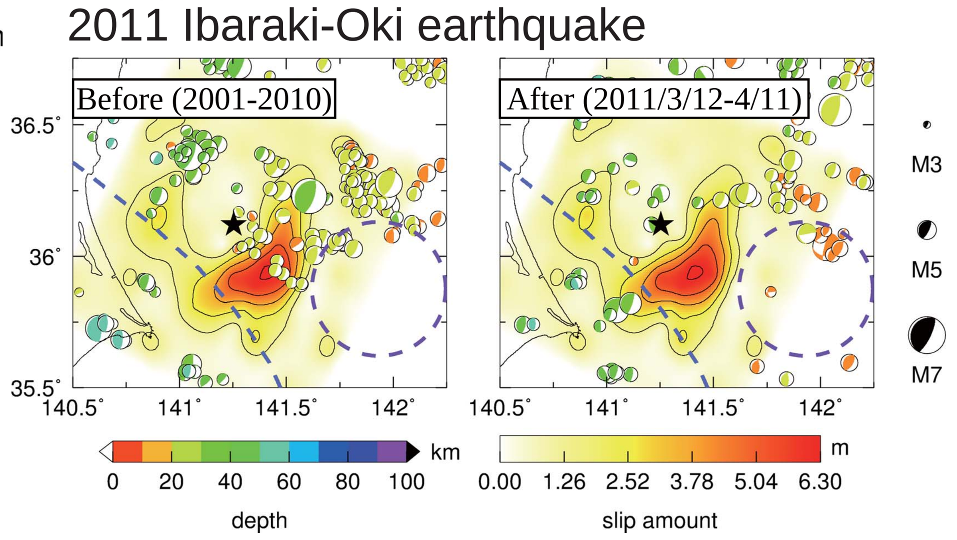

* Spatial distribution of CMTs of the interplate earthquakes (Mw>3.0). These events were selected from F-net CMT solution catalog using the following criteria: 155°≦strike≦245°; 0°≦dip≦ 40°; 45°≦rake≦135°.

This source model indicates that the rupture propagation of the 2011 Ibaraki-Oki earthquake was stopped by the subducted seamount and PHS. This can be understood in the following interpretations:

(1) Because the subducted seamount locally increases the normal stress across the subduction interface and strengthens local interplate coupling (Scholz and Small, 1991), the seamount is expected to work as a rupture "barrier" if the seamount area is not ready for coseismic rupture.

(2) The rupture on the NA-PAC contact zone would be hard to propagate through the PHS-PAC contact zone because of the following condition differences between the NA-PAC and PHS-PAC contact zone: i) Uchida et al. (2009) suggested that the coupling rate in the PHS-PAC contact zone are lower than that in the NA-PAC contact zone. ii) The large afterslip mostly occurred in the PHS-PAC contact zone. This observation and the weak interplate coupling in the PHS-PAC contact zone indicate that the PHS-PAC contact zone would be the compliant area, or slightly velocity-strengthening fault area (Boatwright and Cocco, 1996; Matsuzawa, 2009).

Relationship between the 2011 Tohoku earthquake and the 2011 Ibraki-Oki earthquake

We try to discuss the relationship between the mainshock and the Ibaraki-Oki event in the view points of aftershock occurrence between two events and the after-seismic slip.

Result & Discussion

- Just before the 2011 Ibaraki-Oki earthquake (at 15:03:58 and at 15:07:16), two interplate earthquakes occurred in the northeastern part of the source area of the 2011 Ibaraki-Oki earthquake. Judging from the existence of these events, we can say that the source area of the 2011 Ibaraki-Oki earthquake does not overlap with the large coseismic slip area of the 2011 Tohoku earthquake because aftershocks would occur in the adjacent area to large coseismic slip area.
- Two large after-slip area can be shown and those large after-slip areas do not overlap large coseismic area of the two events. One is located at the deeper side of large coseismic area of the 2011 Tohoku earthquake and the other smaller area is located south side of the coseismic area of the 2011 Ibaraki-Oki earthquake which is found in PAC-PHS contact zone.

■ Interplate aftershocks between the two events

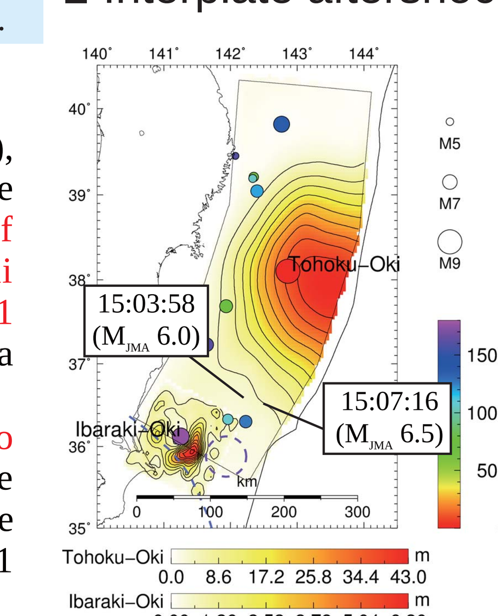

* Circles indicate the epicenters of interplate aftershocks occurred between the mainshock (14:46:18) and the Ibaraki-Oki event (15:15:34). Those events were selected from the JMA catalog, whose hypocenter depths are within ±10km from the PAC-NA plate boundary depth. The colors of the circles indicate the elapsed time from the origin time of the mainshock. We used different color scales of slip distributions for the mainshock and the Ibaraki-Oki event.

■ Co-seismic and after-seismic slip distribution

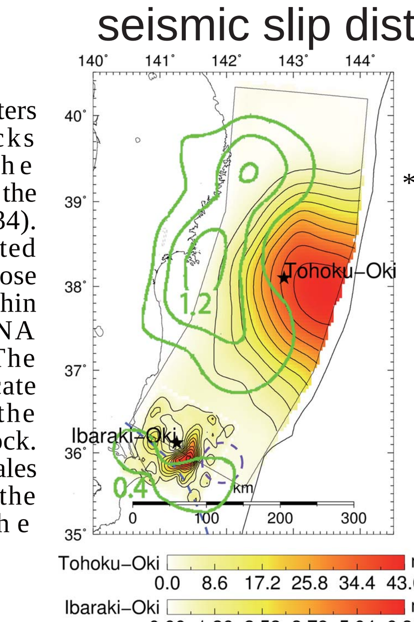

* Afterslip distribution for one month after the 2011 Tohoku earthquake is shown by green contours with 0.4m interval from GPS observations (Ozawa et al., 2011).

Acknowledgement: The strong-motion data recorded by K-NET, KiK-net, and F-net of NIED, the GPS data recorded by GEONET of GSI, the JMA unified hypocenter catalog, and the F-net CMT solution catalog were used for the analysis. The program package by Kikuchi and Kanamori (2003), the program package by Snoke (2009), the program package by Okada (1992), and RTKLIB Ver. 2.4.1 (Takasu, 2011) were also used.

References:
Asano and Iwata (2012), Earth Planets Space, 64, in press.
Boatwright and Cocco (1996), J. Geophys. Res., 101, 895-13,909.
Hartzell and Heaton (1983), Bull. Seismol. Soc. Am., 73, 1553-1583.
Kikuchi, M. and H. Kanamori (2003). http://www.eri.u-tokyo.ac.jp/ETAL/KIKUCHI/.
Kubo and Kakehi (2013), Bull. Seismol. Soc. Am., 103, in press.
Lay et al. (2012), J. Geophys Res., 117, B04311.
Matsuzawa (2009), Journal of the Seismol. Soc. of Japan. 2nd ser., 61, S347-S355.
Mochizuki et al. (2008), Science, 321, 1194-1197.
Ozawa et al. (2012), J. Geophys. Res., 117, B07404.
Sato et al. (2011), Science, 332, 1395.
Scholz and Small (1997), Geology,25, 487-490.
Snoke (2009), Seismol. Res. Lett., 80(2), 260-262.
Takasu (2011), http://www.rtklib.com/.
Uchida et al. (2009), Earth Planet. Sci. Lett., 283, 111-121.

The 2011 Tohoku earthquake

Inversion Detail

Data

Teleseismic body waves

We use the vertical-component waveforms at 42 IRIS stations with epicentral distances in period of 10-100 s containing not only P-phase (where P-phase means direct P-wave and depth phases such as pP and sP) but also PP-phase in this study. The time length of the dataset in the source inversion is 300 s (starting 10 s before the P-wave arrival).

Terrestrial GPS data

We use three components of static displacements at 351 GEONET stations. The static displacements of this event were obtained by differencing its preseismic and postseismic positions.

Seafloor crustal deformation data

We use three components of five seafloor static displacements (Sato et al., 2011).

Green's function

Teleseismic Green's function

P and PP theoretical waveforms are calculated after Kikuchi and Kanamori (2003) with six one-dimensional velocity structure models for subfaults with different locations along the dip direction referring to Miura et al. (2005). Theoretical P and PP phase onsets are set to observed ones for each station.

Geodetic Green's function

Theoretical static displacements were calculated assuming a homogeneous elastic halfspace after Okada (1992).

Method

We use the kinematic linear waveform inversion with multiple time windows (Hartzell and Heaton, 1983). The slip time history of each subfault is represented by the superposition of 24 time windows with 8.0 s width, each of which is put with 4.0 s lag. The maximum slip duration at each subfault (Tsd) of 100 s was determined by semblance analysis of the near-source small-aperture seismic array data of the strong ground motion waveforms to estimate the wave-radiation duration from the area around the hypocenter. We assume a realistic curved fault surface model considering the three-dimensional shape of the plate boundary (Miura et al., 2005; Nakajima and Hasegawa, 2006; Nakajima et al., 2009; Kita et al., 2010). Relative weights among different kinds of data-set were determined by theoretical tests. The propagation velocity of the first time window (Vftw) of 2.0 km/s was determined by the matching of the slip patterns of the teleseismic model and the geodetic model.

Data Fitting

The fitting in both of the teleseismic and geodetic data is quite well. The variance reductions of the teleseismic data and the geodetic data are 67.2% and 99.4%, respectively.

■ Comparison of the observed (red) and synthetic (black) teleseismic body waveforms

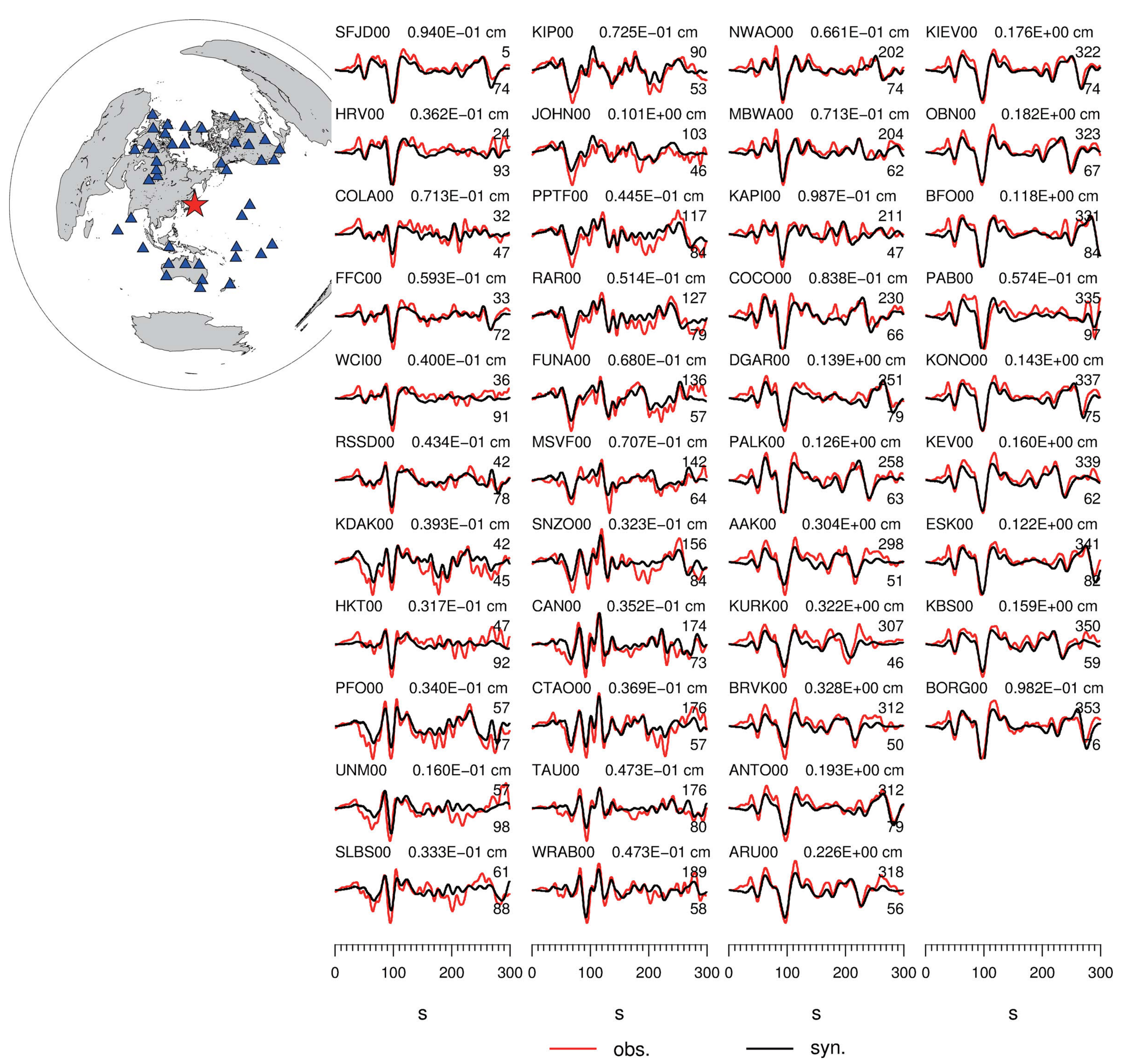

■ Comparison of the observed (red) and synthetic (black) static displacements.

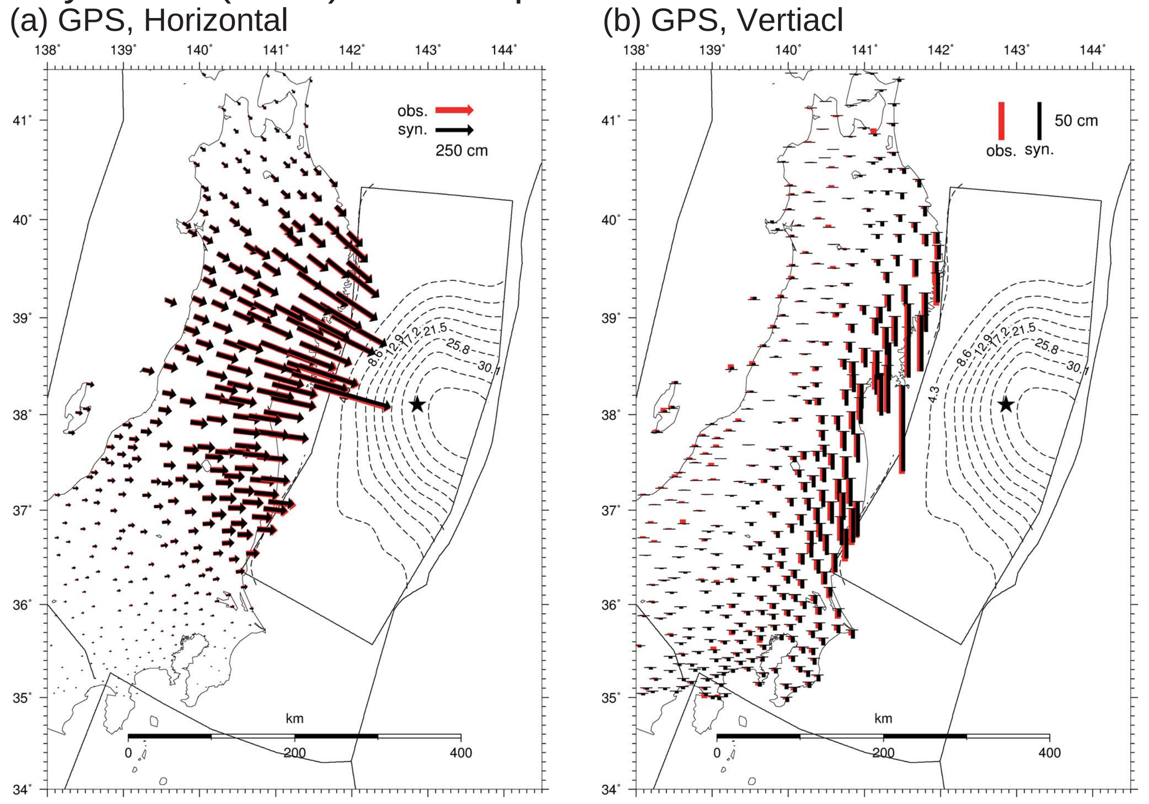

(a) GPS, Horizontal (b) GPS, Vertiacl

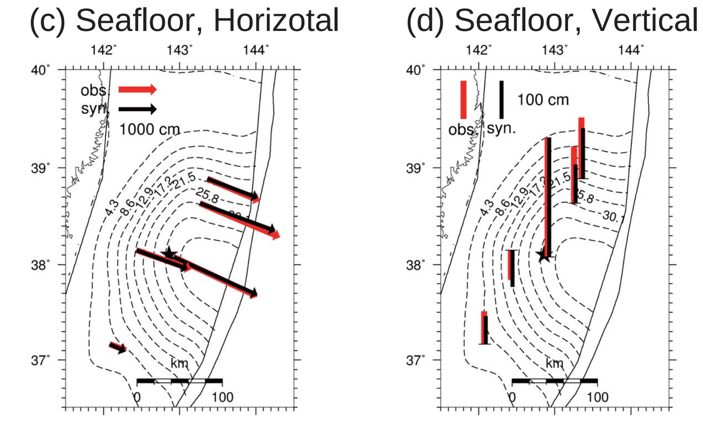

(c) Seafloor, Horizotal (d) Seafloor, Vertical

The 2011 Ibaraki-Oki earthquake

Inversion Detail

Data

Strong-motion data

We use three components of time-series data from the 17 stations (K-NET, KiK-net, and F-net) in period of 5-50 s. The time length of the dataset in the source inversion is 50-80 s (starting 10 s before the S-wave arrival).

GPS data

We use two horizontal components of static displacements at 83 GEONET stations. The static displacements of this event were obtained by differencing its preseismic and postseismic positions.

Green's function

Strong-motion Green's function

Theoretical strong-motion waveforms were calculated using the discrete wavenumber method (Bouchon, 1981) and the reflection/transmission matrix method (Kennet and Kerry, 1979) using one-dimensional velocity structure models for each station referring Japan Integrated Velocity Structure Model Version 1 (Koketsu et al., 2012).

Geodetic Green's function

Theoretical static displacements were calculated assuming a homogeneous elastic halfspace after Okada (1992).

Method

We use the kinematic linear waveform inversion with multiple time windows (Hartzell and Heaton, 1983). The slip time history of each subfault is represented by the superposition of 7 time windows with 4.0 s width, each of which is put with 2.0 s lag. We assume a single planar fault model (120 km along strike × 120 km along dip) with a strike of 206° and a dip of 10° which refers to the spatial distribution of earthquakes deduced from ocean bottom seismographic observations (Yamada et al., 2011). In this study, the relative weights between different kinds of data-set and the relative weight of the smoothing constraint are determined by a trial-and-error process considering the fitting in each data and the agreement between the seismic moment estimated by this analysis and GCMT. The first time window triggering velocity (Vftw) of 2.2 km/s was selected so as to minimize the residual of strong-motion data fitting.

Data Fitting

The fitting in both of the strong-motion and GPS data is quite well. The variance reduction of the strong-motion data and the GPS data are 84.4% and 97.4%, respectively.

■ Comparison of the observed (red) and synthetic (black) strong-motion velocity waveforms

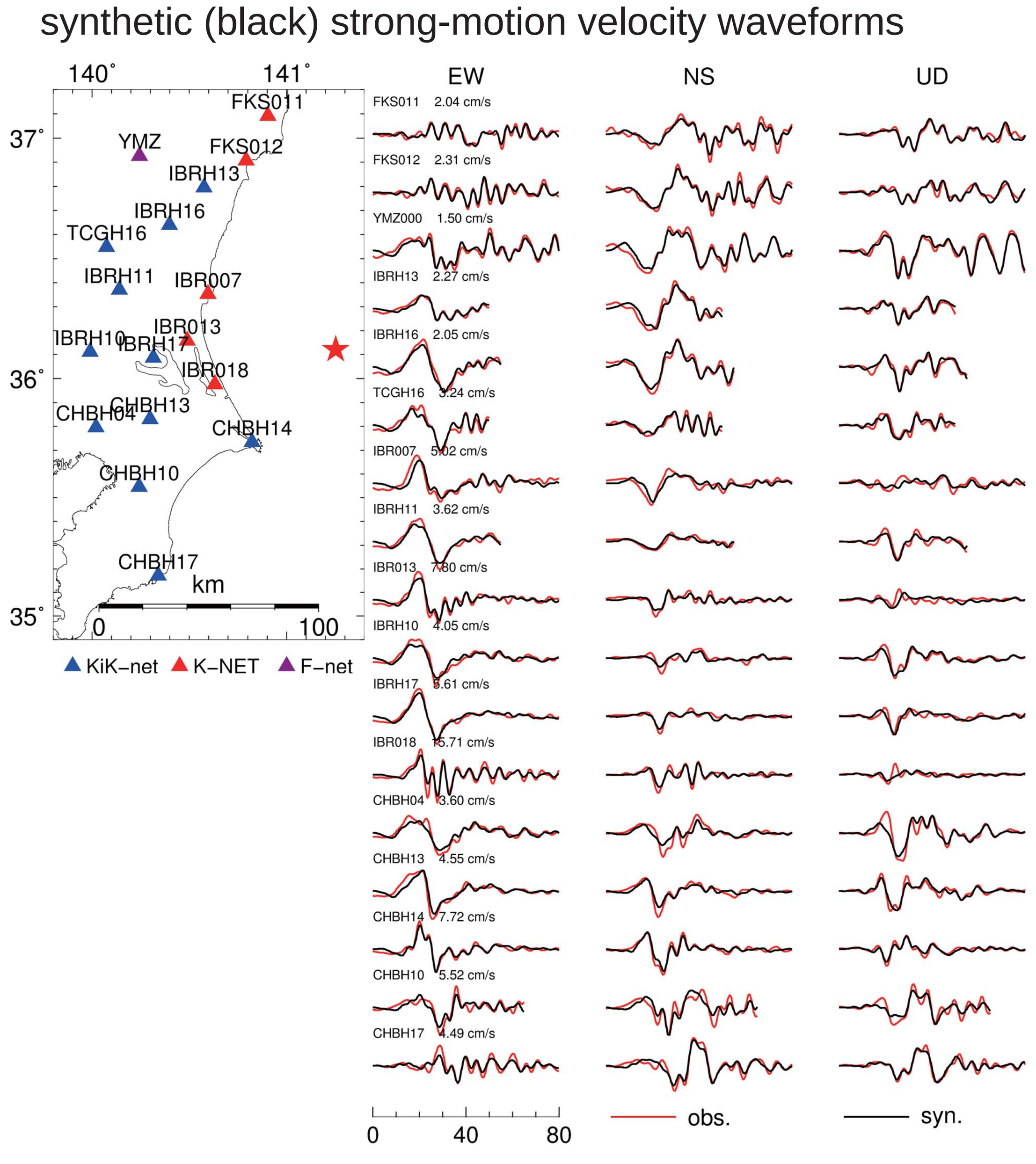

■ Comparison of the observed (red) and synthetic (black) static displacements.

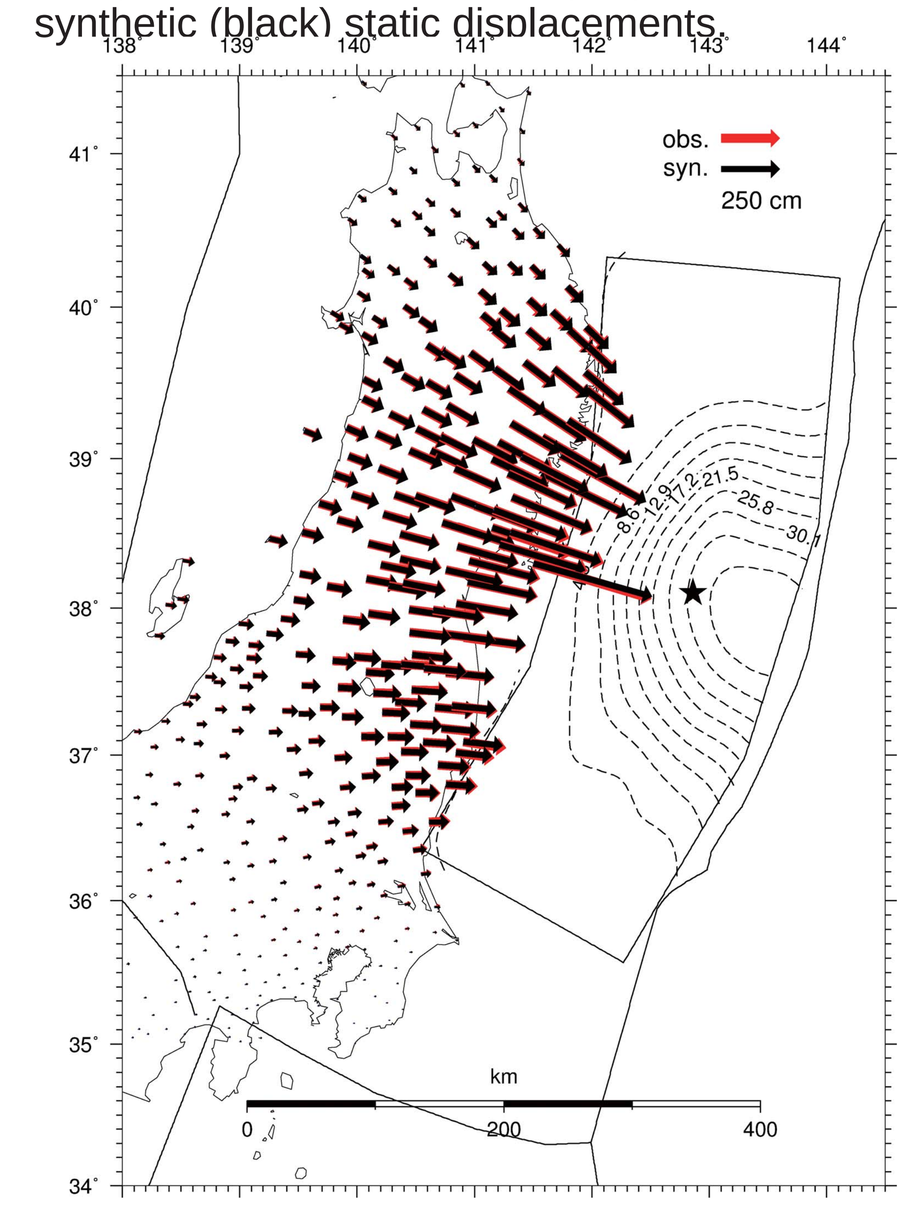

References:

Bouchon (1981), Bull. Seismol. Soc. Am., 71, 959-971.
Hartzell and Heaton (1983), Bull. Seismol. Soc. Am., 73, 1553-1583.
Kennett and Kerry (1979), Geophys. J. R. Astr. Soc., 57, 557-583.
Kikuchi, M. and H. Kanamori (2003). http://www.eri.u-tokyo.ac.jp/ETAL/KIKUCHI/.
Kita et al. (2010), Earth Planet. Sci. Lett., 290, 415-426.
Koketsu et al. (2012), Paper No. 1773 presented at the 15th WCEE.
Miura et al. (2005). Tectonophysics, 407, 165-188.
Nakajima and Hasegawa (2006), Geophys. Res. Lett., 33, L16309.
Nakajima et al. (2009), J. Geophys. Res., 114, B08309.
Okada (1992), Bull. Seismol. Soc. Am., 82, 1018-1040.
Sato et al. (2011), Science, 332, 1395.
Snoke (2009), Seismol. Res. Lett., 80(2), 260-262.
Takasu (2011), http://www.rtklib.com/.
Yamada et al. (2011), Earth Planets Space, 63, 841-845.